Advanced Electrode Homogenization-Based Design of an Electrochemical Pseudo-2D Model for Fast Charging Li-ion Batteries

Raymonda DIAB[a,b,c], Emmanuel SCHAEFFER[a], Philippe POIZOT[b], François AUGER[a], Jean-François COUSSEAU[c]

[a]Nantes Université, Institut de Recherche en Énergie Électrique de Nantes Atlantique, IREENA, UR 4642, F-44600 Saint-Nazaire, France

[b]Nantes Université, CNRS, Institut des Matériaux de Nantes Jean Rouxel, IMN, F-44000 Nantes, France

[c]One-sixone, F-44980 Sainte-Luce-sur-Loire, France

Reducing Li-ion batteries' charging time to 10-15 minutes is currently one of the key challenges for the wide adoption of electric vehicles. However, standard fast-charging methods can shorten battery life and present significant safety risks, including internal short circuits due to Li-plating. To address this issue, we designed an original electrochemical pseudo-2D model that allows online observation of the negative electrode potential, enabling the highest possible charging current to be applied without the risk of Li-plating. Using the concept of electrode homogenization and a non-uniform spatial discretization of the partial differential equations, a non-linear state-space representation can be derived from local electrochemical equations with very few simplifying assumptions. Experimental tests are currently being conducted to calibrate and validate the model using a 3-electrode assembly. This article presents the first results.

Keywords–Lithium-ion battery, Electrochemical model, Fast charging, Reference electrode, Active materials properties, Experimental characterization, Lithium plating.

1. INTRODUCTION

Although technology has significantly advanced, the global uptake of battery electric vehicles (BEVs) continues to face challenges, mainly due to limited driving ranges and long charging times. The reduction of battery charging time to around 10-15 minutes, resulting in 80 % state-of-charge (SOC), has therefore become a priority R&D challenge for several industrial fields, particularly the automotive industry [1, 2]. In fact, this reduction allows, on the one hand, to reduce the cost of vehicle purchase by limiting the required battery storage capacity and, on the other hand, to reduce the time spent at charging stations.

During fast charging, Li ions are extracted from the positive electrode (PE), travel through the electrolyte, and are intercalated into the negative electrode (NE), with a possible reduction to Li metal. This so-called Li plating is one of the major factors that influence the aging and safety performance of Li-ion batteries (LIBs) throughout the fast charging process [3, 4]. Moreover, using standard fast charging protocols can cause safety issues, such as internal short circuits produced by lithium plating at the negative electrode, and reduce the overall lifespan of LIBs [5, 6].

Among existing charging strategies, the constant current-constant voltage (CC-CV) approach remains the industry standard. This protocol prioritizes battery lifespan over speed, preventing its adoption for fast-charging scenarios. Previous studies have shown that monitoring the negative electrode potential during fast charging enables real-time adjustment of the charging strategy to prevent lithium plating and the corresponding capacity fade. Although an additional Li metal reference electrode is required for accurate independent potential measurements in a three-electrode assembly [7, 8, 9]. An alternative approach to monitor the negative electrode (NE) potential involves the use of dedicated models and observers.

Although equivalent circuit models (ECMs) successfully predict terminal voltage behavior, their inability to reconstruct internal electrochemical states, such as the concentrations of lithium ions and electrode potentials, represents a critical gap for applications requiring physical insight into cell operation mechanisms [10]. Physics-based models make a greater knowledge of battery behavior possible. Electrochemical models (EMs) are based on chemical and electrochemical kinetics and transport equations that describe detailed physical phenomena. Unlike equivalent circuit models (ECMs), EMs can provide a physical explanation of the cell's electrochemical behavior and give us access to the potential of the particles near the separator. In fact, these particles have the most negative potential and can give us an indication of the triggering of lithium plating.

However, implementing pseudo-2D (P2D) models for fast-charging simulations presents two core challenges : accurately estimating the numerous physical parameters on many scales (from bulk electrodes to particle interfaces) while ensuring the computational efficiency required for a closed-loop control of the charging current.

These observations form the key motivation behind the presented work. The second section includes the governing equations of the classical P2D model of a Li-ion cell, theoretical notions, assumptions, and the adopted modeling approach. The discretization of the partial differential equations is then carried out, yielding a state-space representation of the model associated with a differential-algebraic equation (DAE) system. In the third section, the experimental procedure of the teardown of a pouch cell and its reconstruction in a three-electrode configuration for parametrization are briefly described. The first simulation results are presented in Section 4 and compared with the experimental data. Finally, the conclusion and future work are drawn in the last section.

2. PHYSICS-BASED MODELING

2.1. *Classical Electrochemical Pseudo-2D Modeling*

Existing P2D models for Li-ion batteries are mainly derived from the model introduced in 1993 by Doyle, Fuller and Newman using a combination of concentrated solution theory and porous electrode theory [11, 12]. Within this modeling approach, solid particles are considered as spheres and the electrode is thought of as the superposition of the solid matrix and the electrolytic phase, both coexisting at all points in the model (Fig. 1). In the electrolyte, c_e is supposed to evolve only in the x direction, representing the spatial direction through the cell thickness, and c_s is considered only in the radial direction in the sphere. The two mediums are interconnected through mass balance equations and reaction kinetics, driven by the potential difference between them. All electrochemical variables of these P2D models are listed in Table A.

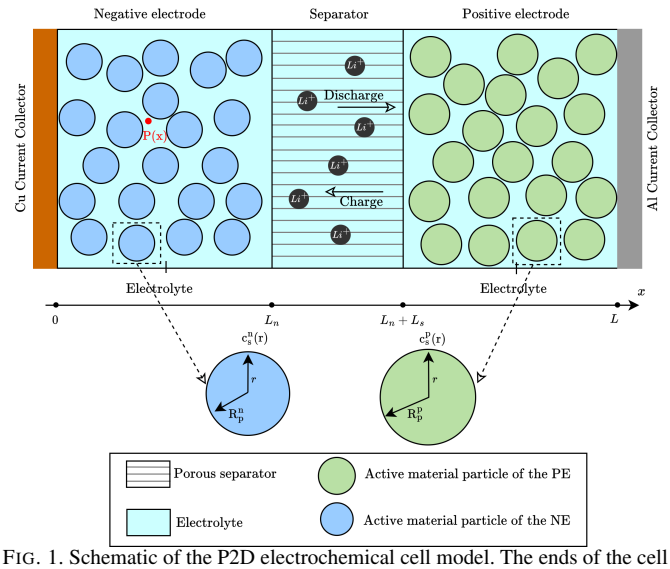

FIG. 1. Schematic of the P2D electrochemical cell model. The ends of the cell are at x = 0 and x = L, where L is the cell thickness.

Although very precise, their computational complexity, derived from coupled nonlinear partial differential equations (PDEs) for mass/charge transport, makes them unsuitable for real-time control or large-scale modeling. Simplified models are therefore effective in situations where computational efficiency is of greater importance than accuracy, but their assumptions fail in fast-charging situations, requiring hybrid approaches or specific adjustments to take electrolyte/thermal effects into account [13, 14]. The prevalence of this challenge drives our research into alternative approaches. The next part introduces and justifies our electrode homogenization-based modeling technique.

2.2. *Homogenized Modeling Approach*

One can observe on scanning electron microscopy (SEM) images [15, 16] that both small and large solid particles coexist within the thickness of the electrodes, alongside the electrolyte. These particles aggregate into clusters of highly different sizes, contradicting one of the main assumptions of conventional P2D models. To reduce computational complexity, we applied electrode homogenization principles to transform the original three-dimensional PDE system into two coupled unidirectional PDEs. This approach, well-established in composite material modeling for electromagnetism and mechanics, enables efficient simulation while preserving essential physics.

Within this framework (illustrated in Figure 2), a Li^+ ion located at the point P(x) in the electrolyte can either continue diffusing through the electrode porosity under the combined influence of the electric field and concentration gradient (Eq. 3), or react at the surface of the nearest active grain and subsequently diffuse through the homogenized solid phase (Eq. 7). We therefore introduce a new dimension, denoted as r, which does not represent the radial direction as in the classical model discussed previously. Instead, it must be considered as the distance, always positive, in the direction in which the lithium particle can diffuse in the equivalent homogenized solid material. Finally, this model operates under only two key simplifying assumptions : uniform solid potential throughout the electrode and isothermal conditions throughout the cell thickness. Li ions are also supposed to move through the electrolyte along the x-axis, whereas electrons in the solid migrate in the same direction.

2.2.1. *Numerical Spatial Discretization*

Numerical models allow for high-resolution simulations, capturing fine details of battery behavior, such as concentration gradients, potential distributions, and local reaction rates. However, differential equations can be difficult to solve analytically and may not be immediately applicable to computer simulations or control algorithms. Commonly used discretization techniques include the finite difference method (FDM) [17, 18], the finite volume method (FVM) [19], and the finite element method (FEM) [20]. In one-dimensional (1D) problems with uniform grids and linear finite elements, the Finite Difference Method (FDM) and Finite Element Method (FEM) yield identical stencil structures and thus equivalent discretized equations for second-order differential operators such as the Poisson equation [21]. For this reason, this work involves discretizing the reformulated battery governing equations at their time and space grid points using the Finite Difference Method (FDM). Boundary and initial conditions are enforced throughout the solution process to maintain the constraints of the equations.

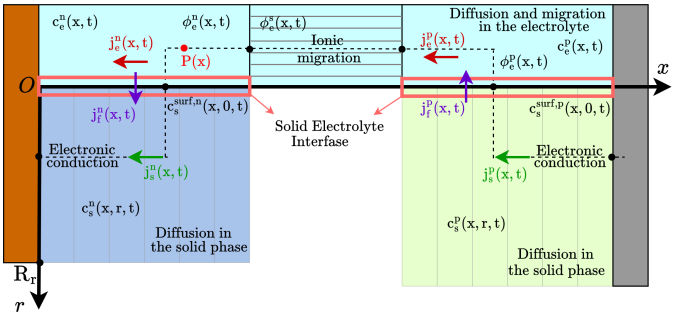

FIG. 2. Homogenization approach of the pseudo-2D model.

Moreover, it is well-known that grid generation plays a critical role in complex simulations. A uniform grid cannot provide a uniform distribution of the discretization error, as the truncation error is affected by both the grid spacing and the variable derivatives [22]. The high density of grid points is found mainly in locations with strong solution activity, such as steep slopes or significant curvature, while larger grid cells are used in smoother solution zones to optimize computing efficiency [23].
In our case, the NE, separator, and PE are not evenly spaced on the x-axis, requiring the use of a non-uniform discretization grid. The cell thickness, L, is divided into N_x grid points with $N_x = N_n + N_s + N_p - 2$, where N_n, N_s and N_p are the number of grid points in the NE, separator and PE, respectively, including the two points for the boundaries on either side of the electrodes. The grid points are indexed by i, with a value of x at a given point i denoted x_i, such that $x_1 = 0$ and $x_{Nx} = L$. The width of the discretization step between x_i and x_{i+1} is represented by h_i.

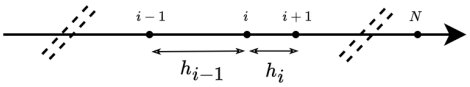

FIG. 3. Finite difference method with non-uniform grid intervals.

Given the dependence of the diffusion coefficient D_e on the electrolyte Li-ion concentration c_e, the diffusion term in Eq. 3 (Table 1) can be expressed as

$$\frac{\partial}{\partial x}\left(D_e^{\text{eff}}(c_e)\,\frac{\partial c_e}{\partial x}(x,t)\right) = \frac{\partial D_e^{\text{eff}}}{\partial c_e}(c_e(x,t))\,\left(\frac{\partial c_e}{\partial x}(x,t)\right)^2 + D_e^{\text{eff}}(c_e(x,t))\,\frac{\partial^2 c_e}{\partial x^2}(x,t) \quad (14)$$

In the following, bold letters refer to vectors that contain the model variables at each point of the grid, for example $\mathbf{c}_e(t) = [c_e(x_1,t),\ldots,c_e(x_{N_x},t)]^T$. All equations of the model given in Table 1 can be vectorized for the model implementation in the

TABLE 1. Li-ion P2D model governing equations.

Mechanisms	Equations	N°	Boundary conditions	N°
Electrode overpotential	$\eta_s^*(x,t) = \phi_s^*(x,t) - \phi_e^*(x,t) - \Psi_s^*(\zeta_s^*(x,t))$	(1)		
Electrochemical kinetics	$j_f^*(x,t) = a_s^*\ i_0^* \left[\exp\left(\frac{\alpha_a\ F}{R\ T}\eta_s^*(x,t)\right) - \exp\left(-\frac{\alpha_c\ F}{R\ T}\eta_s^*(x,t)\right)\right]$	(2)		
Electrolyte phase mass conservation	$\epsilon_e^*\ \frac{\partial c_e^*}{\partial t}(x,t) = \frac{\partial}{\partial x}\left(D_e^{eff,*}\ \frac{\partial c_e^*}{\partial x}(x,t)\right) + \frac{(1-t_+)}{F}\ j_f^*(x,t)$	(3)	$\frac{\partial c_e^n}{\partial x}(0,t) = \frac{\partial c_e^p}{\partial x}(L,t) = 0$	(4)
Electrolyte phase charge conservation	$j_e^*(x,t) = -\kappa_e^{eff,*}\ \frac{\partial \phi_e^*}{\partial x}(x,t) - \kappa_D^{eff,*}\ \frac{\partial}{\partial x}\ln(c_e^*(x,t))$	(5)	$\frac{\partial \phi_e^n}{\partial x}(0,t) = \frac{\partial \phi_e^p}{\partial x}(L,t) = 0$	(6)
Solid phase charge conservation	$j_s^*(x,t) = -\sigma_s^{eff,*}\ \frac{\partial \phi_s^*}{\partial x}(x,t)$	(7)	$\frac{\partial \phi_s^n}{\partial x}(L_n,t) = \frac{\partial \phi_s^p}{\partial x}(L_n+L_s,t) = 0$	(8)
			$-\sigma_s^{eff,n}\ \frac{\partial \phi_s^n}{\partial x}(0,t) = \frac{I(t)}{A^n}$	(9)
			$-\sigma_s^{eff,p}\ \frac{\partial \phi_s^p}{\partial x}(L,t) = \frac{I(t)}{A^p}$	(10)
Solid phase mass conservation	$\frac{\partial c_s^*}{\partial t}(x,r,t) = D_s^*\ \frac{\partial^2 c_s^*}{\partial r^2}(x,r,t)$	(11)	$-D_s^*\ \frac{\partial c_s^*}{\partial r}(x,R_r^*,t) = 0$	(12)
			$-D_s^*\ \frac{\partial c_s^*}{\partial r}(x,0,t) = \frac{{j_f}^*(x,t)}{a_s^*\ F}$	(13)

MATLAB environment. Using this notation, the spatial derivatives of the Li-ion concentration at grid points become :

$$\frac{\partial \mathbf{c}_\mathrm{e}}{\partial x}(t) \approx Dx_1\ .\ \mathbf{c}_\mathrm{e}(t) \tag{14-1}$$

$$\frac{\partial^2 \mathbf{c}_\mathrm{e}}{\partial x^2}(t) \approx Dx_2\ .\ \mathbf{c}_\mathrm{e}(t) \tag{14-2}$$

where $\mathrm{Dx_1}$ and $\mathrm{Dx_2}$ are the spatial discretization matrices derived from [23] and the dot performs standard matrix-vector multiplication. By inserting Equation 14 into the governing equations, we finally obtain a PDAE system.

2.2.2. *Model Implementation*

Upon spatial discretization, partial differential equations are converted into ordinary differential equations (ODEs) and partial differential algebraic equations (PDAEs). Let us note the dynamic state vector $\mathbf{X}$ and the output vector $\mathbf{Y}$ of the ODE problem as :

$$\mathbf{X}(t) = \left[\mathbf{c}_\mathrm{e}(t);\ \mathbf{c}_\mathrm{s}(t)\right] \tag{15}$$

$$\mathbf{Y}(t) = \left[\mathbf{j}_\mathrm{f}(t);\ \boldsymbol{\phi}_\mathrm{s}(t);\ \boldsymbol{\phi}_\mathrm{e}(t);\ \Psi_\mathrm{s}(t);\ \mathbf{j}_\mathrm{s}(t);\ \mathbf{j}_\mathrm{e}(t);\ U(t)\right] \tag{16}$$

where the semicolon (;) corresponds to the MATLAB operator for vector concatenation. By replacing Eq. 14 in Eq. 3 and discretizing Eq. 11 for the two electrodes, respectively, we get the following ODE system where the excitation is the electrochemical reaction rate $\mathbf{j}_\mathrm{f}$:

$$\frac{d\mathbf{c}_\mathrm{e}^n}{dt} = \frac{1}{\epsilon_e^n}\left(\frac{dD_e^{\mathrm{eff,n}}}{d\mathbf{c}_\mathrm{e}^n} * \frac{d\mathbf{c}_\mathrm{e}^n}{dx} * \frac{d\mathbf{c}_\mathrm{e}^n}{dx}\right) + D_e^{\mathrm{eff,n}} * (A_e^n\ .\ \mathbf{c}_\mathrm{e}^n) + B_e^n\ .\ \mathbf{j}_\mathrm{f}^n \tag{17}$$

$$\frac{d\mathbf{c}_\mathrm{e}^s}{dt} = \frac{1}{\epsilon_e^s}\left(\frac{dD_e^{\mathrm{eff,s}}}{d\mathbf{c}_\mathrm{e}^s} * \frac{d\mathbf{c}_\mathrm{e}^s}{dx} * \frac{d\mathbf{c}_\mathrm{e}^s}{dx}\right) + D_e^{\mathrm{eff,s}} * (A_e^s\ .\ \mathbf{c}_\mathrm{e}^s) \tag{18}$$

$$\frac{d\mathbf{c}_\mathrm{e}^p}{dt} = \frac{1}{\epsilon_e^p}\left(\frac{dD_e^{\mathrm{eff,p}}}{d\mathbf{c}_\mathrm{e}^p} * \frac{d\mathbf{c}_\mathrm{e}^p}{dx} * \frac{d\mathbf{c}_\mathrm{e}^p}{dx}\right) + D_e^{\mathrm{eff,p}} * (A_e^p\ .\ \mathbf{c}_\mathrm{e}^p) + B_e^p\ .\ \mathbf{j}_\mathrm{f}^p \tag{19}$$

$$\frac{d\mathbf{c}_\mathrm{s}^n}{dt} = A_s^n\ .\ \mathbf{c}_\mathrm{s}^n + B_s^n\ .\ \mathbf{j}_\mathrm{f}^n \tag{20}$$

$$\frac{d\mathbf{c}_\mathrm{s}^p}{dt} = A_s^p\ .\ \mathbf{c}_\mathrm{s}^p + B_s^p\ .\ \mathbf{j}_\mathrm{f}^p \tag{21}$$

where the symbol $*$ refers to the element-wise multiplication in MATLAB. The state matrices $\mathrm{A_e^{n,s,p}}$, $\mathrm{B_e^{n,s,p}}$, $\mathrm{A_s^{n,p}}$ and $\mathrm{B_s^{n,p}}$ include lumped values and are calculated as follows :

$$A_e^{n,s,p} = \frac{1}{\epsilon_e^{n,s,p}}\ Dx_2 \quad , \quad B_e^{n,s,p} = \frac{(1-t_+)}{F\ \epsilon_e^{n,s,p}}$$

$$A_s^{n,p} = D_s^{n,p}\ \frac{1}{(\Delta r_{n,p})^2}\begin{bmatrix} -2 & 2 & 0 & \cdots & \cdots & 0 \\ 1 & -2 & 1 & \ddots & & \vdots \\ 0 & 1 & -2 & \ddots & \ddots & \vdots \\ \vdots & \ddots & \ddots & \ddots & \ddots & 0 \\ \vdots & & \ddots & 1 & -2 & 1 \\ 0 & \cdots & \cdots & 0 & 2 & -2 \end{bmatrix}$$

$$B_s^{n,p} = \frac{2}{a_s^{n,p} \cdot F \cdot h_{n,p}}$$

Finally, we obtain the following semi-explicit system :

$$\text{ODE system :} \quad \frac{d\mathbf{X}}{dt}(t) = f\left(\mathbf{X}(t), \mathbf{j}_\mathrm{f}(t)\right) \tag{22}$$

$$\text{DAE system :} \quad 0 = g\left(\mathbf{X}(t), \mathbf{j}_\mathrm{f}(t), I(t)\right) \tag{23}$$

where the DAE system results from considering the boundary conditions 9, 10 and 13 of discretized equations 7 and 11. The diagram shown in Fig. 4 models this dynamic PDAE-ODE system with feedback loops that ensure coupled behavior. Electrode homogenization simplifies Eq. 23 to a root-finding problem involving two scalar functions (one per electrode).

3. EXPERIMENTAL WORK

Accurate simulation of the behavior of Li-ion batteries requires detailed knowledge of the open-circuit potential of each electrode. To achieve this, an industrial pouch cell was drained to 0 % state of charge (SOC) using a C/10 constant current discharge to 2.75 V, and dismantled in an argon environment to prevent unwanted film formation on electrodes due to air contact. The experimental procedure involved cell disassembly and reconstruction into a three-electrode PAT-Cell configuration consisting of two 18 mm diameter perforated electrodes, a 21.6 mm diameter industrial separator together with 100 μL of

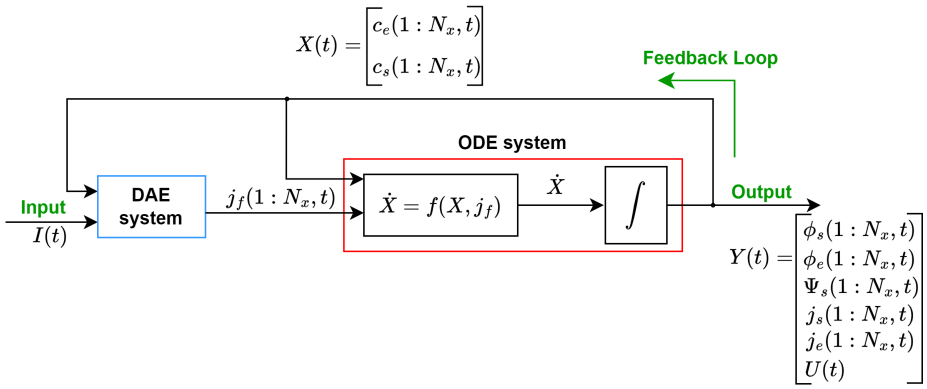

FIG. 4. Block diagram of the proposed P2D model. Here X is the state vector and the spatial coordinates along the thickness of the cell are represented as 1 :N_x.

electrolyte, and a metal lithium ring as the reference electrode (Figure C). The PAT-Cell was next subjected to a sequence of pulses at a constant current of C/20 for an increase in SOC of 2 %, and then left to rest until an equilibrium condition was satisfied. This electrochemical characterization was performed to determine the open-circuit potential (OCP) of individual electrodes. Consequently, constant current charge/discharge excitations were performed for different C-rates to estimate the model parameters.

4. RESULTS AND DISCUSSION

One fundamental limitation of single-particle (SP) models is their assumption of uniform, time-invariant solution-phase concentration. Figure 5(a) demonstrates how our proposed model captures the spatio-temporal evolution of the electrolyte concentration within the cell thickness during a 2C CC charge. The observed curve shape exhibits strong agreement with results obtained from alternative simulation tools [24]. Figure 5(b) reveals significant electrolyte potential gradients that SP models also inherently neglect. Our proposed modeling approach explicitly incorporates these solution-phase dynamics, enabling a reliable prediction of high C-rate performance. The time-dependent electrode potential assumption in SP models is shown to maintain validity at high rates, as demonstrated in Figure 5(c) and previously validated by K. Rahimian et al. for 5C [25].

The model enables visualization of the critical C-rate threshold for Li-plating (LP) initiation and reveals that this degradation phenomenon begins near the separator beyond a critical C-rate, quantified here for 8C charging (Figure 6). This side reaction occurs when

$$\eta_{\mathrm{LP}} = \phi_s(L_n, t) - \phi_e(L_n, t) \leq 0$$

where η_{LP} is the overpotential of this side reaction.

Simulations with the P2D model were compared with experimental data to validate the dynamics of the model and the selection of parameters. The experimental data come from measurements performed on PAT-Cells. The first results are shown in Figure 7. While the present simulation demonstrates generally good agreement with experimental results, slight discrepancies persist due to the limited tuning of two key parameters. These will be more precisely estimated by implementing advanced optimization techniques benchmarked against prior experimental data.

5. CONCLUSION

This article presents the first results obtained with an electrochemical P2D model dedicated to fast charging of Li-ion batteries. The ability of the model to remain numerically stable at very high current results from the electrode homogenization process. Experiments have been conducted with three-electrode PAT-Cells to estimate the model parameters, which are cell-dependent. Now, parameter estimation will be carried out to fit the simulation to the experimental data and therefore to improve the model's accuracy. Future work will focus on the design and implementation of a robust fast-charging algorithm to control the charging current in real time, based on online observation of the negative electrode potential.

6. REFERENCES

[1] Mussa, A. S. et al., "Fast-charging to a partial state of charge in lithium-ion batteries : A comparative ageing study", Journal of Energy Storage, vol. 13, pp. 325–333, 2017. https://www.sciencedirect.com/science/article/pii/S2352152X17301913.

[2] Ye, Y. et al., "Effect of thermal contact resistances on fast charging of large format lithium ion batteries", Electrochimica Acta, Vol. 134, pp. 327-337, (2014), https://www.sciencedirect.com/science/article/pii/S0013468614008949.

[3] Fleischhammer, M. et al., "Interaction of cyclic ageing at high-rate and low temperatures and safety in lithium-ion batteries", Journal of Power Sources, Vol. 274, pp. 432-439, (2015), https://www.sciencedirect.com/science/article/pii/S037877531401489X.

[4] Iturrondobeitia, A. et al., "Post-Mortem Analysis of Calendar-Aged 16 Ah NMC/Graphite Pouch Cells for EV Application", The Journal of Physical Chemistry C, Vol. 121, pp. 2186521876, (2017), https://pubs.acs.org/doi/10.1021/acs.jpcc.7b05416.

[5] Zhang, S.S. et al., "Study of the charging process of a LiCoO2-based Li-ion battery", Journal of Power Sources, Vol. 160, pp. 1349-1354, (2006), https://www.sciencedirect.com/science/article/pii/S0378775306004162.

[6] Edge, J. S. et al., "Lithium ion battery degradation : what you need to know", Physical Chemistry Chemical Physics, Vol. 23, pp. 8200–8221, (2021), https://pubs.rsc.org/en/content/articlelanding/2021/cp/d1cp00359c.

[7] Chu, Z. et al., "Non-destructive fast charging algorithm of lithium-ion batteries based on the control-oriented electrochemical model", Applied Energy, Vol. 204, pp. 1240-1250, (2017), https://www.sciencedirect.com/science/article/pii/S0306261917303501.

[8] Waldmann, T. et al., "Optimization of Charging Strategy by Prevention of Lithium Deposition on Anodes in high-energy Lithium-ion Batteries – Electrochemical Experiments", Electrochimica Acta, Vol. 178, pp. 525-532, (2015), https://www.sciencedirect.com/science/article/pii/S0013468615303066.

[9] Dotoli, M. et al., "Detection of Lithium Plating in Li-Ion Cell Anodes Using Realistic Automotive Fast-Charge Profiles", Batteries, Vol. 7, pp. 46, (2021), https://www.sciencedirect.com/science/article/pii/S0013468615303066.

[10] Zhang, X. et al., "A novel method for identification of lithium-ion battery equivalent circuit model parameters considering electrochemical properties", Journal of Power Sources, Vol. 345, pp. 21-29, (2017), https://www.sciencedirect.com/science/article/pii/S0378775317301295.

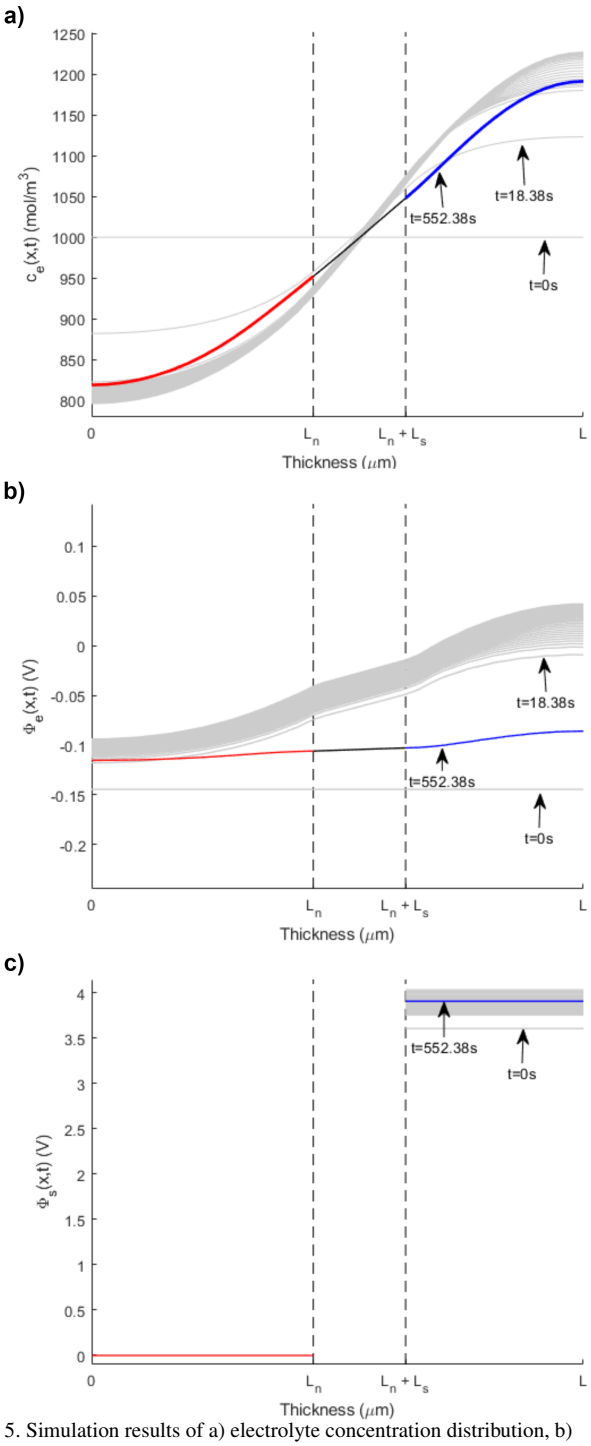

FIG. 5. Simulation results of a) electrolyte concentration distribution, b) electrolyte potential and c) solid potential inside the cell during 2C CC charging as a function of the cell thickness. Each line represents a distinct time evolution.

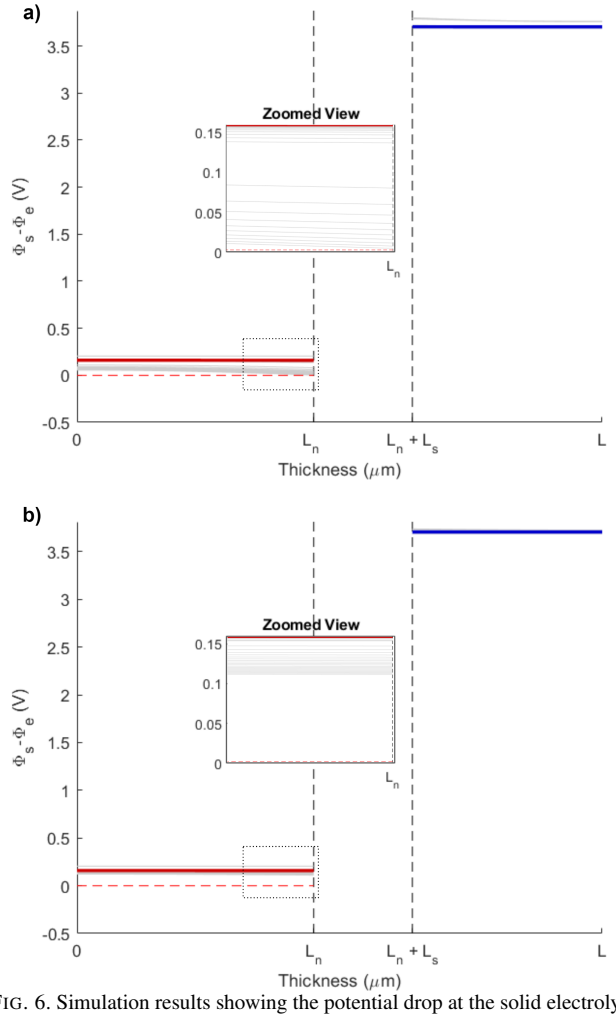

FIG. 6. Simulation results showing the potential drop at the solid electrolyte interface (SEI) between the negative electrode and the electrolyte detecting Li-plating onset : (a) high-rate (8C) vs. (b) moderate (2C) CC charge simulations.

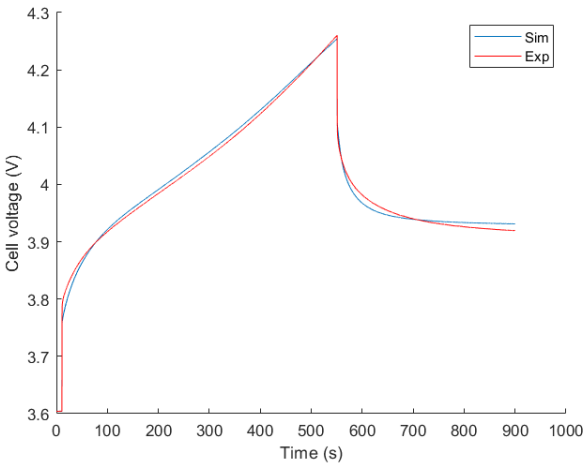

FIG. 7. Comparison between the proposed P2D model simulations and the experimental data for 2C CC charge.

[11] Doyle, M. et al., “Modeling of Galvanostatic Charge and Discharge of the Lithium/Polymer/Insertion Cell", Journal of The Electrochemical Society, Vol. 140, pp. 1526, (1993), https://iopscience.iop.org/article/10.1149/1.2221597/meta.

[12] Newman, J. and Tiedemann, W., “Porous-electrode theory with battery applications", AIChE Journal, Vol. 21, pp. 25-41, (1975), https://onlinelibrary.wiley.com/doi/abs/10.1002/aic.690210103.

[13] Zhang, Q. et al., “Capacity fade analysis of a lithium ion cell", Journal of Power Sources, Vol. 179, pp. 793-798, (2008), https://www.sciencedirect.com/science/article/pii/S0378775308001134.

[14] Moura, S. et al., ‘Battery State Estimation for a Single Particle Model With Electrolyte Dynamics", IEEE Transactions on Control Systems Technology, Vol. 25, pp. 453-468, (2017), https://ieeexplore.ieee.org/abstract/document/7489035.

[15] Chen, C. et al., « Development of Experimental Techniques for Parameterization of Multi-scale Lithium-ion Battery Models», Journal of The Electrochemical Society, Vol. 167, pp. 080534, (2020), https://dx.doi.org/10.1149/1945-7111/ab9050.

[16] Nickol, A. et al, “GITT Analysis of Lithium Insertion Cathodes for Determining the Lithium Diffusion Coefficient at Low Temperature : Challenges and Pitfalls", Journal of The Electrochemical Society, Vol. 167, pp. 090546, (2020), https://dx.doi.org/10.1149/1945-7111/ab9404.

[17] Pramanik, S. et al., “Electrochemical model based charge optimization for lithium-ion batteries", Journal of Power Sources, Vol. 313, pp. 164-177, (2016), https://www.sciencedirect.com/science/article/pii/S0378775316300969.

[18] Seong Beom, L. et al., “A Robust and Sleek Electrochemical Battery Model Implementation : A MATLAB® Framework", Journal of The Electrochemical Society, Vol. 168, pp. 090527, (2021), https://dx.doi.org/10.1149/1945-7111/ac22c8.

[19] Ashwin, T.R. et al., “Modified electrochemical parameter estimation of NCR18650BD battery using implicit finite volume method", Journal of Power Sources, Vol. 341, pp. 387-395, (2017), https://www.sciencedirect.com/science/article/pii/S0378775316317062.

[20] Hu, X. et al., “A linear time-invariant model for solid-phase diffusion in physics-based lithium ion cell models", Journal of Power Sources, Vol. 214, pp. 40-50, (2012), https://www.sciencedirect.com/science/article/pii/S0378775312007720.

[21] LeVeque, Randall J., “Finite Difference Methods for Ordinary and Partial Differential Equations", SIAM : Philadelphia, PA, (2007), https://doi.org/10.1137/1.9780898717839.

[22] Seoul National University, “Lecture Notes on Numerical Methods," (2015), https://ocw.snu.ac.kr/sites/default/files/NOTE/4090.pdf.

[23] Veldman, A.E.P. et al., “Playing with nonuniform grids", Journal of Engineering Mathematics, Vol. 26, pp. 119-130, (1992), https://doi.org/10.1007/BF00043231.

[24] Torchio, M. et al., « LIONSIMBA : A MATLAB Framework Based on a Finite Volume Model Suitable for Li-Ion Battery Design, Simulation, and Control», Journal of The Electrochemical Society, Vol. 163, pp. A1192, (2016), https://iopscience.iop.org/article/10.1149/2.0291607jes/meta.

[25] Rahimian, S. K. et al., « Extension of physics-based single particle model for higher charge-discharge rates», Journal of Power Sources, Vol. 224, pp. 180-194, (2013), https://www.sciencedirect.com/science/article/pii/S0378775312015054

[26] PAT-Cell | Cableless 3-Electrode Battery Test Cell. (2016, January 21). Retrieved from https://www.el-cell.com/products/test-cells/standard-test-cells/pat-cell/

A. LIST OF VARIABLES OF THE P2D MODEL

Symbol	Variables (Units)
c_e	Li ion concentration in the electrolyte (mol/m^3)
c_s	Li ion concentration in the electrode (mol/m^3)
ϕ_e	Electrolyte potential (V)
ϕ_s	Electrode potential (V)
j_e	Electrolyte current density (A/m^2)
j_s	Electrode current density (A/m^2)
i_0	Exchange current density (A/m^2)
I(t)	Input current (A)
U(t)	Output voltage (V)
j_f	Electrochemical reaction rate (A/m^3)
η_s	Surface overpotential (V)
ζ_s	Insertion rate at the surface of an electrode (-)
Ψ_s	Open circuit potential of an electrode (V)

B. LIST OF SYMBOLS

Symbol	Description (Units)
a_s	Specific interfacial area (m^{-1})
c_e^0	Initial lithium ion concentration (mol/m^3)
c_s^0	Initial lithium concentration (mol/m^3)
c_s^{max}	Maximum lithium concentration (mol/m^3)
D_e	Intrinsic electrolyte diffusion coefficient (m^2/s)
D_e^{eff}	Effective electrolyte diffusion coefficient (m^2/s)
D_s	Diffusion coefficient in active material of electrode (m^2/s)
K_e	Electrolyte ionic conductivity (S/m)
K_e^{eff}	Effective electrolyte ionic conductivity (S/m)
L	Thickness of domain (m)
r	Dimension through the solid phase of electrodes (m)
R_p	Solid particle radius (m)
R_r	Equivalent distance into the solid particles (m)
t	Time (s)
T	Temperature (K)
x	Dimension through thickness of electrodes (m)
ϵ_e	Porosity or void volume fraction of the electrolyte (-)
ϵ_s	Porosity or void volume fraction of the active material (-)
κ	Intercalation rate constant $(m^{2.5}/mol^{0.5}s)$
φ_s	The flux density inside active material particles (mol/m^2s)
σ_s	Electronic conductivity (S/m)

C. PAT-CELL

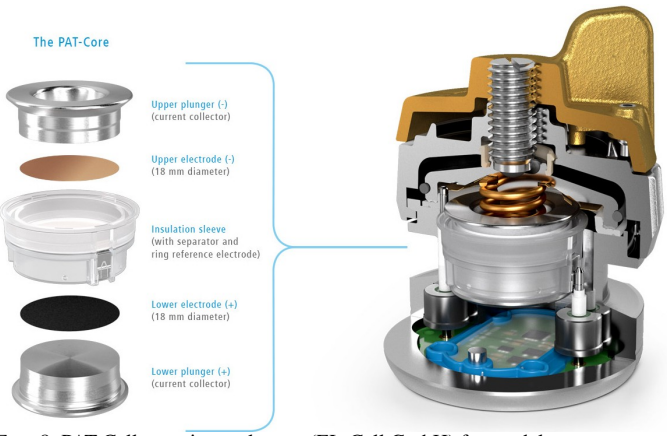

FIG. 8. PAT-Cell experimental setup (EL-Cell GmbH) for model parameterization and validation. The configuration employs single-sided coated electrodes with an integrated ring reference electrode positioned within the separator, enabling individual electrode potential measurements. Source : EL-Cell GmbH [26]